# On energy harvesting using piezoelectric transducer with two-port model under force excitation

Rafael Tavares
*University of Agder (UiA)*
*Faculty of Engineering and Science*
Grimstad, Norway
rafael.tavares@uia.no

Michael Ruderman
*University of Agder (UiA)*
*Faculty of Engineering and Science*
Grimstad, Norway
michael.ruderman@uia.no

*Abstract*—Piezoelectric (PE) materials are functional materials that can be used for transforming mechanical stress into electrical energy, that can then be stored and used for powering another devices. In this paper, we provide experimental investigation of PE transducers used for energy harvesting under external force-controlled excitation. The lumped parameter electromechanical model (LPEM) has been assumed and brought into a generalized two-port network notation. Laboratory experiments using an universal test machine (UTM) were performed and used for the parameter identification of the model. The two-port model formulation is validated by comparing results of numerical simulations and experimental data. A numerical analysis of power conversion between the mechanical and electrical domains and potential energy harvesting capabilities of the PE transducer under stress are presented based on the experimental results.

*Index Terms*—piezoelectric transducer, two-port model, energy harvesting, system identification, electromechanical model

## I. INTRODUCTION

Piezoelectric (PE) materials have been used in actuation systems requiring precision in nano-positioning and force control, such as micromanipulators, micro-valves, atomic force microscopes, adaptive optics, ultra-precision machine tools and structure dampers [1], [2]. PE materials are favorable due to being compact, light-weight and with high precision and high bandwidth response [2].

Despite being mostly known for their use as actuators, the piezoelectric effect exhibited by these materials can be divided into two direct and converse effects. When an electric field is applied between the electrodes, it produces a mechanical strain which can be used for actuation and positioning (converse effect). A PE material produces an electric potential when strained (direct effect), which can be used for sensing applications, such as in electro-acoustic transducers, pressure sensors in touch pads or tilt sensors in consumer electronics [3].

Over the last decades, PE materials have been actively researched also in energy harvesting applications, mainly due to their high actuation frequency range, high power density and bidirectional coupling between mechanical and electrical properties. For an extensive overview of the use of PE materials in energy harvesting applications we refer to [4]–[9].

The most conventional description of the piezoelectricity was published by the standards committee of the IEEE [10]

as linearized constitutive equations

$$S_i = s_{ij}^E T_j + d_{ki} E_k, \qquad (1)$$

$$D_i = d_{ik} T_j + \varepsilon_{ik}^T E_k. \qquad (2)$$

The constitutive equations state that the material strain $S_i$ and electrical displacement $D_i$ are linearly related to the mechanical stress $T_j$ and the electrical field $E_k$. The piezoelectric charge $d$, permittivity $\varepsilon$ and elastic compliance $s$ are the material constants, the $i$ and $j$ subscripts indicate the directions of displacement and polarization. The superscripts $E$ and $T$ denote that constants are evaluated at constant electric field and constant stress, respectively. Despite describing uniformly the general relationship between the electrical and the mechanical domain, these equations lack to capture both nonlinearities and dynamic transients observed in PE actuators and transducers, such as rate-independent hysteresis, creep and vibrations. Furthermore, these constitutive coefficients can turn out as temperature-dependent and show a strong electric field dependency.

Different modeling approaches have been proposed in the literature for the electromechanical behavior of PE materials, see [1] and references within. Some models do not decouple different dynamics and physical effects, are only valid over small frequency ranges and neglect other effects such as creep and vibration dynamics. In order to account both forward and feedback interaction between the electrical and mechanical domains (both direct and converse PE effects), a physics or domain-oriented modeling approach is needed to obtain an electromechanical comprehensive model as referred e.g. in [2], [3].

Some models follow a cascade model structure, where decoupled sub-models are used to model hysteresis, creep, and vibration dynamics effects, and connected to form a comprehensive model of the PE. Also, due to the cascading connection between the sub-models, this model structure is very suitable for implementing control schemes with their inverse models. Although, cascade model approaches mostly take into consideration one-way coupling, since they are rather control-oriented approximations [2]. For applications envisaging the simultaneous energy harvesting and damping control of the PE transducer, a physical electromechanical interpretation

that can be compatible with a two-port network model [11] and capable of incorporating a two-way PE coupling effects is needed.

A most notable approach was introduced by the lumped parameter electromechanical model (LPEM) proposed in [12], [13], managing to postulate the nonintuitive behavioral phenomena evidenced by PE actuators. A more detailed view of the LPEM model and its inclusion in the two-port network model is later described in Section II. An extended lumped parameter was proposed in [14] where state-varying capacitance and Voigt-Kelvin-type linear creep effects were incorporated into LPEM model and have been experimentally demonstrated on a standard commercial PE stack actuator.

This paper provides experimental investigation of PE element used for the energy harvesting under the force-controlled external excitation. The LPEM model has been brought into a generalized two-port network notation and identified from a series of dedicated experiments on an universal test machine (UTM). In particular, for mechanical excitation cycles we measure and analyze the harvested energy output of the PE element under stress. The paper is organized as follows. In Section II we summarize the implemented two-port model based on the LPEM including hysteresis. The experimental setup for PE excitation and measurements is described in Section III. The analysis of the experimental results, parameter identification, power and energy estimation are discussed in Section IV and the paper is summarized in Section V.

## II. SYSTEM DESCRIPTION

### A. Lumped parameter electromechanical model

Before formulating the two-port network for the PE transducer we briefly summarize the lumped parameter electromechanical model [12], [13]. The lumped parameter consideration leads to ordinary differential equations describing the system dynamical behavior. Assuming the PE transducer as a one-mass $m$ with stiffness $k$ and damping $b$, the mechanical domain is governed by the differential equation

$$m\ddot{x} + b\dot{x} + kx = F_t + F, \tag{3}$$

where $F_t$ represents the transduced force from electrical domain and $F$ the external mechanical force.

Since PE materials are dielectric, the electric domain is mainly governed by a capacitive behavior. Experimental observations show rate-independent hysteresis exhibited between voltage and displacement as well as between force and displacement. Since there is no hysteresis when with open leads, but it is rather observed when closed leads between displacement and charge, this allows to postulate that the net electrical charge $q_p$ across the PE is given by the sum of two components

$$q_p = q_c + q_t \tag{4}$$

where the component $q_c$ results from the voltage across the capacitor and is defined by

$$q_c = Cv_t, \tag{5}$$

where $C$ is the electrical capacitance of the PE. Due to the direct PE effect, there is a coupled charge induced by the mechanical domain because of the relative displacement $x$. Also, due to the converse PE effect, there is a transduced force from the electrical domain proportional to the capacitor voltage. Considering the constant transformer ratio $T$, the electromechanical coupling between both domains is given by

$$q_t = Tx, \tag{6}$$

$$F_t = Tv_t. \tag{7}$$

Rate-independent hysteresis lies solely in the electrical domain, between the applied actuator voltage and resulting charge [12], introducing the non-linearities into the electrical domain that can be expressed as

$$v_h = H(q). \tag{8}$$

From Kirchhoff's second law, the overall voltage between electrodes of the PE is given by

$$v_p = v_t + v_h. \tag{9}$$

Note that one of the outputs of the electromechanical model is the charge $q_p$, which is generally challenging to measure. The resulting current $i_p = \dot{q}_p$ is flowing through the PE transducer when the circuit is closed.

### B. Two-port network model

A transducer converts energy from the source domain into another energy (sink) domain. PE transducers have one port in the mechanical domain and one in the electrical domain.

Generic two-port network transducer models can be applicable for most types of reciprocal power conserving transducers, in particular for electrostatic, piezoelectric, electromagnetic and electrodynamic transducers [11], [15]. A standard two-port model of a transducer can be defined by the input across and through variables and the respectively output variables. The across variable for an electrical element is voltage and the through variable is current (or charge). The across variable for mechanical element is force and the through variable is velocity. The power can be then obtained by multiplying the across and through variables.

A simple linear two-port PE transducer can be formulated directly from linear constitutive equations (1) and (2)

$$\begin{bmatrix} S \\ D \end{bmatrix} = \begin{bmatrix} s & d \\ d & \varepsilon \end{bmatrix} \begin{bmatrix} T \\ E \end{bmatrix} \tag{10}$$

and was used in [11] to formulate an estimation of the maximum output power and efficiency of the system. But here one should consider that a PE transducer two-port model is a bidirectionally coupled $2 \times 2$ multi-input-multi-output (MIMO) system which is nonlinear, in general terms. Therefore, our goal is to derive a two-port model, which describes both actuating and sensing transducer effects coupled between the electrical and mechanical domains, and that relying on the prime, to say physics-based, principle of the PE.

From the LPEM equations (3-9) it is possible to map the PE transducer that couples the electrical and mechanical domains, as shown in Fig. 1.
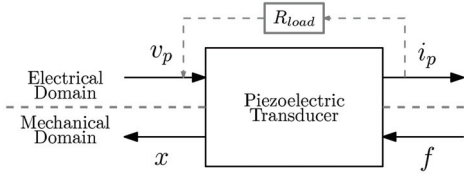
Fig. 1: Two-port network model for the PE transducer.

## C. Hysteresis behavior

The Maxwell-slip model structure used to describe the voltage-charge hysteresis in [12], [14] coincides with the Prandtl-Ishlinskii (P-I) stop-type hysteresis [16]. It resides in the electrical domain and relates the transducers electrical voltage to charge. In the implemented two-port network model, the rate-independent hysteresis is inversely modeled as

$$q_p = H^{-1}(v_h) \qquad (11)$$

and therefore implemented using the P-I play-type operator. This operator is well-known in mechanics and often used for describing the kinematic play, also known as backlash. It provides a multi-valued rate-independent map under a common input $\dot{v}$ into each operator. The play-type hysteresis operator dynamics can be described in a differential form [16] as

$$\dot{q} = \begin{cases} \dot{v} & \text{if} \quad q - r = v \vee q + r = v \\ 0 & \text{if} \quad q - r < v < q + r \end{cases}. \qquad (12)$$

The P-I hysteresis models show a fast analytical computation in both forward and inverse hysteresis models. Using the superposition of play-type operators as schematically illustrated in Fig. 2, it is possible to sufficiently map the real hysteresis by relatively small number of free parameters.
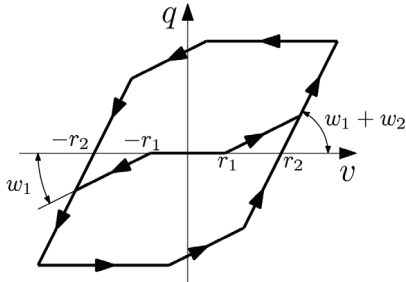


Fig. 2: Schematic representation of P-I play-type model with two operators.

## D. Energy harvesting

Vibration suppression and energy harvesting of a PE transducer can be done by shunting the free leads to an impedance [17]. A typical energy harvesting circuit for the PE element consists in a AC-DC full rectifying bridge with an output capacitor [4], [18]. That is however subject to our future works, since in this paper we use a passive load to estimate the potential energy harvesting output of the transducer under force loads. Due to the bidirectional coupling, the PE transducer can

convert energy from the mechanical to the electrical domain and vice versa. The energy conversion in the PE transducer reveals how much of the potential power supplied by the vibrations actually gets converted to electricity. The conversion efficiency is commonly given by

$$\eta = \frac{P_{out}}{P_{in}}, \qquad (13)$$

where $P_{out}$ is the electrical power output and $P_{in}$ is the mechanical power supplied by the force excitation [15]:

$$P_{mec} = F\dot{x} \quad \text{and} \quad P_{ele} = v_p i_p. \qquad (14)$$

The energy can be obtained by numerical integration of equations (14). The energy losses dissipated in the PE transducer due to damping and coupling effects can be expressed by

$$E_{mec} = E_{ele} + E_{loss}. \qquad (15)$$

## III. EXPERIMENTAL SETUP

The experimental setup consists of a PE transducer under compressive load excitation. During the experiments, four variables are being monitored: the force excitation $F$ applied to the PE, the relative displacement $x$, the voltage $v_p$ across the two electrodes of the PE and the current $i_p$ flowing through the closed circuit.

The measuring circuit includes a resistive load and a shunt resistance ($R_{shunt} = 100\Omega$) for current measurement as shown in Fig. 3. A current sense amplifier was used to increase the voltage output of the current shunt resistance (TI INA213) as the measured voltage $v_{sense}$ with an amplification factor of 50. Two other operational amplifiers (AD8510) were used as buffers for measuring the voltage between the electrode ends of the PE stack. Three different impedances were used as load: $R_1 = 51.43k\Omega$, $R_2 = 97.78k\Omega$ and $R_3 = 143.8k\Omega$.
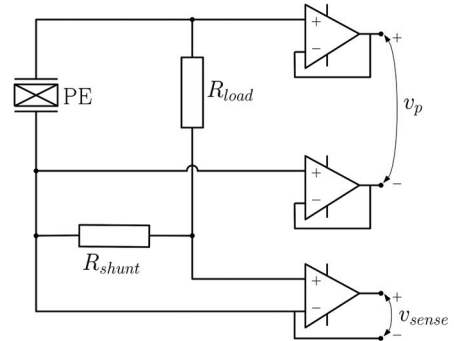


Fig. 3: Electronic circuit for voltage and current measurement.

The specimen was tested using an UTM from SI-Plan. Several load experiments were conducted under compression using two types of the force loads: step and sinusoidal. The experiments carried out under step load profiles consist in a step force applied during 5 seconds, followed by the release of the force. Experiments were carried out with different loads $F_{step} = \{0.50, 0.75, 1.00, 1.25\}$ kN. The experiments with sinusoidal load profile were conducted under different maximum peak forces $F_{max} = \{0.50, 0.75, 1.00, 1.25, 1.50\}$

kN , and for different frequencies $f = \{1; 2; 3; 4; 5\}$. A minimum peak force offset around 0.1kN was applied to avoid loss of mechanical contact due to no compression forces.

The force measurements were provided by the load cell installed in the servo-hydraulic actuator of the UTM (Si-Plan S8390 load cell, rating: ± 25kN, sensitivity 0.593mV/V, 700Ω bridge), from the analog voltage output and the corresponding calibration curve for determining the offset voltage for zero load. The relative displacement, which corresponds to the stroke of the PE, is measured by a laser-optical displacement sensor configured in direct reflection mode (Micro-Epsilon ILD2300-2, Measuring Range: 2mm, Resolution: 0.03$\mu$m). This sensor provides a configurable analog voltage output through the C-Box conditioning signal unit. A 3D-printed frame was produced to allow the adjustment of the measurement range and the fixture of the sensor to the bottom frame of the machine. The analog signals monitored during the experiments were collected using a dSpace MicroLabBox through standard BNC connectors. The analog measuring input channels have a voltage range of ±10V followed by an ADC with a resolution of 16bit and the sampling rate was set to 1kHz. To guarantee the load distribution over the PE surface and minimize the effects of small misalignments between the top clamp with bottom frame of the machine, the load was applied into a sphere joint and then transferred to the PE through a steel rod. An additional metal plate was added to create a reflection surface for the laser beam. The laboratory view of the implemented PE setup under load excitation in the UTM is shown in Fig. 4.
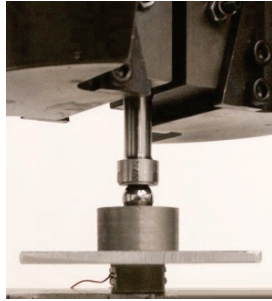


Fig. 4: Laboratory view of the PE in the UTM.

## IV. EXPERIMENTAL RESULTS AND DISCUSSION

The measured relative displacement or stroke $x$, current $i_p$ and voltage $v_p$ during the two force load experiments are depicted in Fig. 5 and Fig. 6. The voltage and current peaks resulting from the step force load reflect the charge flowing through the PE caused by the change of polarization due to mechanical stress. The output current voltage is also a symmetrical sinusoidal signal under sinusoidal load. The hysteresis between voltage and displacement as well as between force and displacement cf. with [12], [13] were observed. From sinusoidal load excitation under different frequencies, one sees that for low frequencies (1-5 Hz) the hysteresis is rate-independent, as shown in Fig. 7.
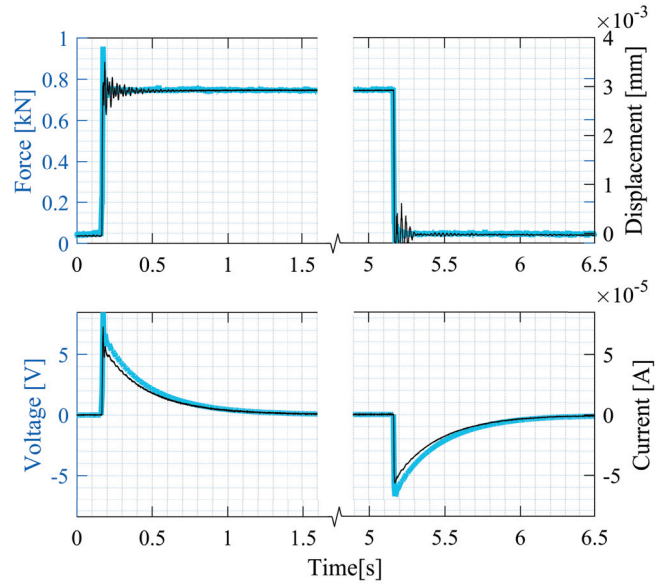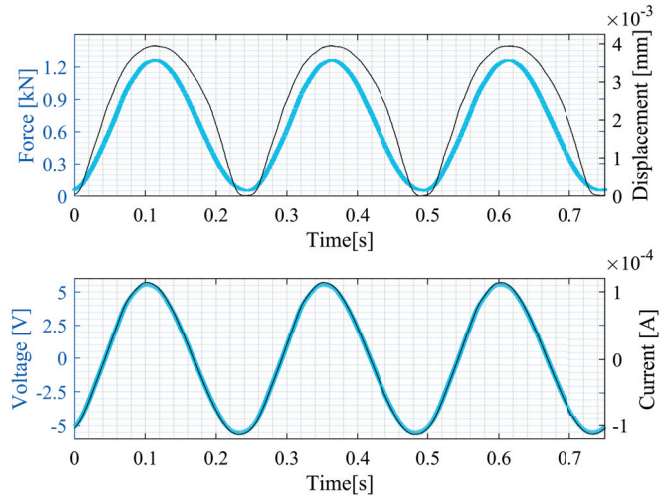


Fig. 5: PE under a step load excitation



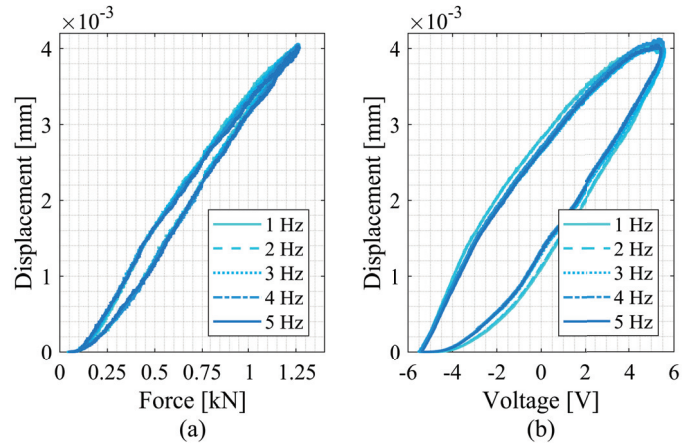Fig. 6: PE under a sinusoidal load excitation



Fig. 7: Measured hysteresis: (a) Displacement-Force; (b) Displacement-Voltage.

## A. Power and energy analysis

From eq. (15), one can estimate the average electrical energy that can be harvested per cycle (one cycle considers the step load and step unload) and the corresponding power peaks. Newton-Cotes Simpson's rule was used for the discrete numerical integration of the electrical power output. The average values from the different experiment conditions are listed in Tables I and II.

TABLE I: Average $E_{ele}$/cycle and $P_{ele}$ peak under step force excitation

| Force (kN) | $R_{load}$ (k$\Omega$) | $E_{ele}$/cycle (mJ) | $P_{ele}$ peak (mW) |
|---|---|---|---|
| 0.50 | 51.43 | 0.594 | 0.579 |
| 0.50 | 97.78 | 0.519 | 0.339 |
| 0.50 | 143.8 | 0.470 | 0.257 |
| 0.75 | 51.43 | 1.397 | 1.484 |
| 0.75 | 97.78 | 1.213 | 0.856 |
| 0.75 | 143.8 | 1.090 | 0.634 |
| 1.00 | 51.43 | 2.450 | 2.386 |
| 1.00 | 97.78 | 2.123 | 1.366 |
| 1.00 | 143.8 | 1.908 | 0.996 |

TABLE II: Average $E_{ele}$/cycle and $P_{ele}$ peak under sinusoidal force excitation

| f (Hz) | F = 0.5kN | | F = 0.75kN | | F = 1kN | |
|---|---|---|---|---|---|---|
| | $E_{ele/cycle}$ (mJ) | $P_{ele\,peak}$ (mW) | $E_{ele/cycle}$ (mJ) | $P_{ele\,peak}$ (mW) | $E_{ele/cycle}$ (mJ) | $P_{ele\,peak}$ (mW) |
| 1 | 0.22 | 0.04 | 0.57 | 0.12 | 1.02 | 0.21 |
| 2 | 0.34 | 0.08 | 0.94 | 0.21 | 1.70 | 0.36 |
| 3 | 0.39 | 0.08 | 1.20 | 0.25 | 1.93 | 0.39 |
| 4 | 0.41 | 0.09 | 1.26 | 0.26 | 2.02 | 0.41 |
| 5 | 0.42 | 0.09 | 1.28 | 0.26 | 2.08 | 0.42 |

The velocity $\dot{x}$ was obtained via numeric differentiation. A Butterworth 3$^{\text{rd}}$ order low-pass filter with cut-off frequency of 100Hz was applied to $\dot{x}$ to remove the effects of derivate signal noise. The same filter was applied to force $F$ to introduce the same phase lag, therefore calculating $P_{mec}$ and $E_{mec}$ shown in Tables III and IV.

In the sinusoidal force solicitation, it is noticeable that the harvesting potential saturates as the frequency increases, due to the resistive circuit load. The harvesting potential can be increased using synchronized switch harvesting on inductor (SSHI) techniques [19], [20], which consist in adding up a switching circuit in parallel with the PE element. In SSHI harvesting methods, the PE voltage is always increasing, except during the switch which inverts the PE voltage at each peak, and has always the same sign as the velocity $\dot{x}$.

The power dissipated by the load resistance is small when compared with the power provided by the mechanical load excitation. The PE shunt-damping introduced by the resistance $R_{load}$ reduces the mechanical vibration and, consequently, the total harvested energy. The load impedance needs to be tuned to the shunt-circuit resonant frequency of the system to increase the harvesting power.

## B. Parameter identification

The two-port model was parameterized for a commercially available PE ring stack transducer (Noliac NAC2125-H10).

TABLE III: Average $E_{mec}$/cycle and $P_{mec}$ peak under step force excitation

| Force (kN) | $R_{load}$ (k$\Omega$) | $E_{ele}$/cycle (mJ) | $P_{ele}$ peak (mW) |
|---|---|---|---|
| 0.50 | 51.43 | 15.241 | 24.623 |
| 0.50 | 97.78 | 15.163 | 24.655 |
| 0.50 | 143.8 | 15.540 | 25.111 |
| 0.75 | 51.43 | 31.997 | 46.927 |
| 0.75 | 97.78 | 28.925 | 47.124 |
| 0.75 | 143.8 | 29.246 | 48.172 |
| 1.00 | 51.43 | 45.359 | 73.847 |
| 1.00 | 97.78 | 44.665 | 77.284 |
| 1.00 | 143.8 | 44.807 | 76.928 |

TABLE IV: Average $E_{mec}$/cycle and $P_{mec}$ peak under sinusoidal force excitation

| f (Hz) | F = 0.5kN | | F = 0.75kN | | F = 1kN | |
|---|---|---|---|---|---|---|
| | $E_{mec/cycle}$ (mJ) | $P_{mec\,peak}$ (mW) | $E_{mec/cycle}$ (mJ) | $P_{mec\,peak}$ (mW) | $E_{mec/cycle}$ (mJ) | $P_{mec\,peak}$ (mW) |
| 1 | 11.01 | 2.57 | 20.80 | 4.20 | 31.14 | 6.78 |
| 2 | 21.11 | 4.33 | 41.34 | 8.29 | 61.94 | 12.52 |
| 3 | 32.04 | 6.39 | 65.24 | 12.60 | 92.34 | 18.84 |
| 4 | 42.91 | 8.32 | 88.67 | 18.95 | 123.14 | 26.17 |
| 5 | 53.81 | 11.01 | 112.59 | 24.68 | 155.62 | 34.43 |

The mass was calculated from the geometry and density of the material. The mechanical stiffness was calculated using the blocking force and free endpoint displacement to the rated voltage. From the open-lead stiffness and the charge and voltage constants, one is able to estimate an initial value for the electromechanical coupling $T$. The linear electrical capacitance C is provided in the supplier datasheet. The initial damping coefficient $b$ value was based on previous works, assuming the same critical damping [12].

The measurements from different force and frequency of sinusoidal loads were used for identifying the hysteresis behavior of PE transducer. The sinusoidal load frequencies $f$ are very low when compared with the high resonating frequency of the PE transducer. P-I hysteresis model was discretized with $n = 3$ elements. The $r_i$ and $w_i$ parameters for the correspondent deadband width and slope have been identified simultaneously with the damping coefficient $b$ and transformer ratio $T$. The parameter identification used the minimization of

$$\min \int \left[ \left( i(t) - \hat{i}(t) \right)^2 + \left( x(t) - \hat{x}(t) \right)^2 \right] dt \qquad (16)$$

where $\hat{i}(t)$ and $\hat{x}(t)$ are two-port model estimated outputs for current and displacement, respectively. The determined system parameters are listed in Table V.

The comparisons of the experimental responses of the PE transducers and two-port model simulation responses are represented in Fig. 8 and Fig. 9 for the step and sinusoidal loads.

## V. SUMMARY

In this work, a two-port network model of a PE transducer has been implemented and the model parameters were identified with experimental data. The model was based on the lumped parameter electromechanical one [12] and couples the

TABLE V: Determined system parameters

| Variable | Description | Value | Units |
|---|---|---|---|
| $m$ | Mass | 0.0158 | kg |
| $b$ | Damping coefficient | 1250 | Ns/m |
| $k$ | Stiffness coefficient | $3.125 \times 10^8$ | Ns/m |
| $R_{load}$ | Load impedance | 97.78 | k$\Omega$ |
| $C$ | Capacitance | 3.2 | $\mu$F |
| $T$ | Electromechanical coupling | 7.822 | - |
| $r_1$ | P-I operator 1 threshold | 0.1 | $\mu$F |
| $r_2$ | P-I operator 2 threshold | 0.3 | $\mu$F |
| $r_3$ | P-I operator 3 threshold | 0.7 | $\mu$F |
| $w_1$ | P-I operator 1 slope | 0.5 | V/$\mu$F |
| $w_2$ | P-I operator 2 slope | 1.5 | V/$\mu$F |
| $w_3$ | P-I operator 3 slope | 0.5 | V/$\mu$F |
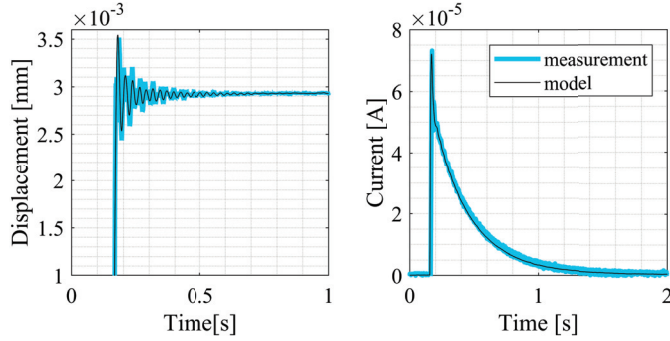


Fig. 8: Measured and Two-Port predicted displacement and current response to a step load ($F_{step} = 1.25$kN).
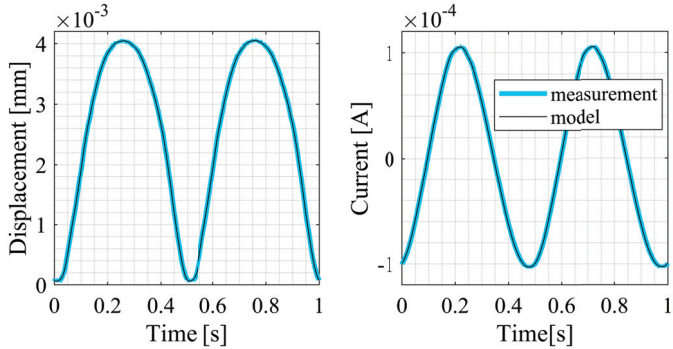


Fig. 9: Measured and Two-Port predicted displacement and current response to a sinusoidal load ($F_{step} = 1.25$kN and $f = 2$Hz).

electrical and mechanical domains in both directions. Experimental measurements allowed to observe the hysteric behavior on the electrical domain. The two-port network model was evaluated by comparing results of numerical simulations and experimental data under the direct PE effect. The analysis of the power in the electrical domain demonstrates the capabilities of PE transducers to harvest sufficient energy to power small electronic circuits, even though the applied resistive load was not optimal. SSHI energy harvesting strategies should be further investigated.

An accurate prediction of both mechanical and electrical output variables by the derived two-port network model argues in favor of its further use in analysis and design of a PE-

based energy harvesting system, which principal feasibility was confirmed in this experimental investigation.

### REFERENCES

[1] G.-Y. Gu, L.-M. Zhu, C.-Y. Su, H. Ding, and S. Fatikow, "Modeling and control of piezo-actuated nanopositioning stages: A survey," *IEEE Transactions on Automation Science and Engineering*, vol. 13, pp. 313–332, 2016.

[2] A. J. Fleming and K. K. Leang, *Design, modeling and control of nanopositioning systems*. Springer, 2014.

[3] S. J. Rupitsch, *Piezoelectric Sensors and Actuators: Fundamentals and Applications*. Springer, 2018.

[4] G. K. Ottman, H. F. Hofmann, A. C. Bhatt, and G. A. Lesieutre, "Adaptive piezoelectric energy harvesting circuit for wireless remote power supply," *IEEE Transactions on power electronics*, vol. 17, no. 5, pp. 669–676, 2002.

[5] H. A. Sodano, D. J. Inman, and G. Park, "Comparison of piezoelectric energy harvesting devices for recharging batteries," *Journal of intelligent material systems and structures*, vol. 16, no. 10, pp. 799–807, 2005.

[6] S. R. Anton and H. A. Sodano, "A review of power harvesting using piezoelectric materials (2003–2006)," *Smart materials and Structures*, vol. 16(3):R1, 2007.

[7] Y. Shu and I. Lien, "Analysis of power output for piezoelectric energy harvesting systems," *Smart materials and structures*, vol. 15, no. 6, p. 1499, 2006.

[8] Y. Liu, G. Tian, Y. Wang, J. Lin, Q. Zhang, and H. F. Hofmann, "Active piezoelectric energy harvesting: general principle and experimental demonstration," *Journal of Intelligent Material Systems and Structures*, vol. 20, no. 5, pp. 575–585, 2009.

[9] R. Caliò, U. B. Rongala, D. Camboni, M. Milazzo, C. Stefanini, G. De Petris, and C. M. Oddo, "Piezoelectric energy harvesting solutions," *Sensors*, vol. 14, no. 3, pp. 4755–4790, 2014.

[10] "IEEE standard on piezoelectricity," *ANSI/IEEE Std 176-1987*, 1988.

[11] S. Roundy, "On the effectiveness of vibration-based energy harvesting," *Journal of intelligent material systems and structures*, vol. 16, no. 10, pp. 809–823, 2005.

[12] M. Goldfarb and N. Celanovic, "A lumped parameter electromechanical model for describing the nonlinear behavior of piezoelectric actuators," *Journal of dynamic systems, measurement, and control*, vol. 119, no. 3, pp. 478–485, 1997.

[13] ——, "Modeling piezoelectric stack actuators for control of micromanipulation," *IEEE control systems*, vol. 17, no. 3, pp. 69–79, 1997.

[14] M. Ruderman, Y. Kamiya, and M. Iwasaki, "Extended lumped parameter electromechanical model of piezoelectric actuators," *2015 IEEE International Conference on Mechatronics, ICM 2015*, pp. 290–295, 04 2015.

[15] K. Janschek, "The generic mechatronic transducer model–a unified system modeling approach," *IFAC Proceedings Volumes*, vol. 43, no. 18, pp. 267–276, 2010.

[16] M. Ruderman and D. Rachinskii, "Use of prandtl-ishlinskii hysteresis operators for coulomb friction modeling with presliding," in *Journal of Physics: Conference Series*, vol. 811, no. 1. IOP Publishing, 2017, p. 012013.

[17] Z. Jin-qiu, P. Zhi-zhao, Z. Lei, and Z. Yu, "A review on energy-regenerative suspension systems for vehicles," in *Proceedings of the world congress on engineering*, vol. 3, 2013, pp. 3–5.

[18] L. Zuo and P.-S. Zhang, "Energy harvesting, ride comfort, and road handling of regenerative vehicle suspensions," *Journal of Vibration and Acoustics*, vol. 135, no. 1, p. 011002, 2013.

[19] Y. Wang and D. J. Inman, "A survey of control strategies for simultaneous vibration suppression and energy harvesting via piezoceramics," *Journal of Intelligent Material Systems and Structures*, vol. 23, no. 18, pp. 2021–2037, 2012.

[20] H. Li, C. Tian, and Z. D. Deng, "Energy harvesting from low frequency applications using piezoelectric materials," *Applied physics reviews*, vol. 1, no. 4, p. 041301, 2014.